NANO LETTERS
Cite This: Nano Lett. 2018, 18, 7870−7875
Letter
pubs.acs.org/NanoLett

Favorable Core/Shell Interface within Co_2P/Pt Nanorods for Oxygen Reduction Electrocatalysis

Chang Liu,[†] Zhong Ma,[‡] Meiyang Cui,[†] Zhiyong Zhang,[†] Xu Zhang,[§] Dong Su,[∥] Christopher B. Murray,[⊥] Jia X. Wang,[‡] and Sen Zhang*[,†]

[†]Department of Chemistry, University of Virginia, Charlottesville, Virginia 22904, United States
[‡]Chemistry Division, Energy and Photon Sciences Directorate, Brookhaven National Laboratory, Upton, New York 11973, United States
[§]Department of Physics and Astronomy, California State University Northridge, Northridge, California 91330, United States
[∥]Center for Functional Nanomaterials, Brookhaven National Laboratory, Upton, New York 11973, United States
[⊥]Department of Chemistry, University of Pennsylvania, Philadelphia, Pennsylvania 19104, United States

Supporting Information

ABSTRACT: Nanostructures with nonprecious metal cores and Pt ultrathin shells are recognized as promising catalysts for oxygen reduction reaction (ORR) to enhance Pt efficiency through core/shell interfacial strain and ligand effects. However, core/shell interaction within a real catalyst is complex and due to the presence of various interfaces in all three dimensions is often oversimply interpreted. Using Co_2P/Pt core/shell structure as a model catalyst, we demonstrate, through density functional theory (DFT) calculations that forming $Co_2P(001)/Pt(111)$ interface can greatly improve Pt energetics for ORR, while $Co_2P(010)/Pt(111)$ is highly detrimental to ORR catalysis. We develop a seed-mediated approach to core/shell Co_2P/Pt nanorods (NRs) within which $Co_2P(001)/Pt(111)$ interface is selectively expressed over the side facets and the undesired $Co_2P(010)/Pt(111)$ interface is minimized. The resultant Co_2P/Pt NRs are highly efficient in catalyzing ORR in acid, superior to benchmark CoPt alloy and Pt nanoparticle catalyst. As the first example of one-dimensional (1D) core/shell nanostructure with an ultrathin Pt shell and a nonprecious element core, this strategy could be generalized to develop ultralow-loading precious-metal catalysts with favorable core/shell interactions for ORR and beyond.

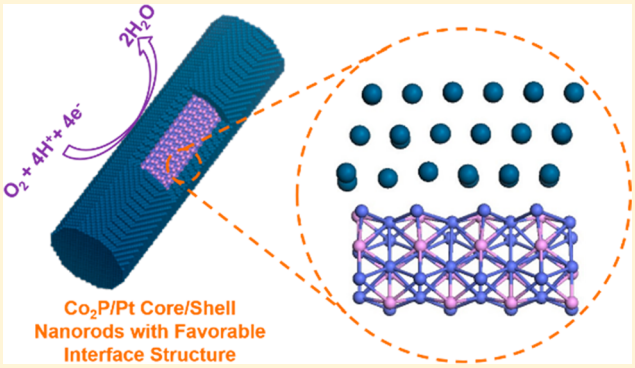

KEYWORDS: *Core/shell, interface, nanorod, oxygen reduction, seed-mediated synthesis*

Advanced polymer electrolyte membrane fuel cells (PEMFCs) for transportation and stationary grid applications demand the development of cost-effective oxygen reduction reaction (ORR) cathodic catalysts with the desired catalytic activity and durability.[1,2] Pt-based materials, a primary choice of catalyst for ORR in the acid electrolytes, have been extensively studied to satisfy this demand during the past two decades.[3,4] Many efforts have been concentrated on Pt-based nanoparticles (NPs) with precisely controlled physical architectures to improve Pt utilization efficiency and intrinsic catalytic property.[5−7] For example, choosing proper transition metals (M, for example, Co, Ni, Fe, and rare-earth metals) to alloy with Pt NPs can modify Pt d-band position or width, leading to improved Pt binding energetics to oxygenate intermediates and therefore enhanced ORR activity.[8−17] To preferentially expose Pt(111) surface, one favorable and thermodynamically stable crystal plane identified by single crystalline model catalyst study, PtM alloy NPs primarily bounded by Pt (111) facets, such as octahedral[16,18−22] and icosahedral[23] NPs and ultrathin nanowires,[24,25] have been synthesized and exhibited appealing ORR performance. Furthermore, to make NPs surfaces highly accessible to reactant, Pt and PtM hollow and porous nanoframes or nanocages have also been designed and constructed.[26−28] One common feature shared by all these catalysts, either intentionally created or self-evolved during catalysis, is that they present a core/shell-like structure with a Pt ultrathin shell (Pt-skin or Pt surface segregation, normally less than 1 nm) promoted by the underlying PtM alloy cores, as M is hardly stabilized in the NPs surface in acid.

Core/shell enhancement can be induced by the interfacial ligand and strain effects.[29−34] In principle, the former is a result of the charge transfer between core and shell components,[35] whereas the latter originates from compressive/tensile strain

Received: September 10, 2018
Revised: November 5, 2018
Published: November 14, 2018

DOI: 10.1021/acs.nanolett.8b03666
Nano Lett. 2018, 18, 7870−7875

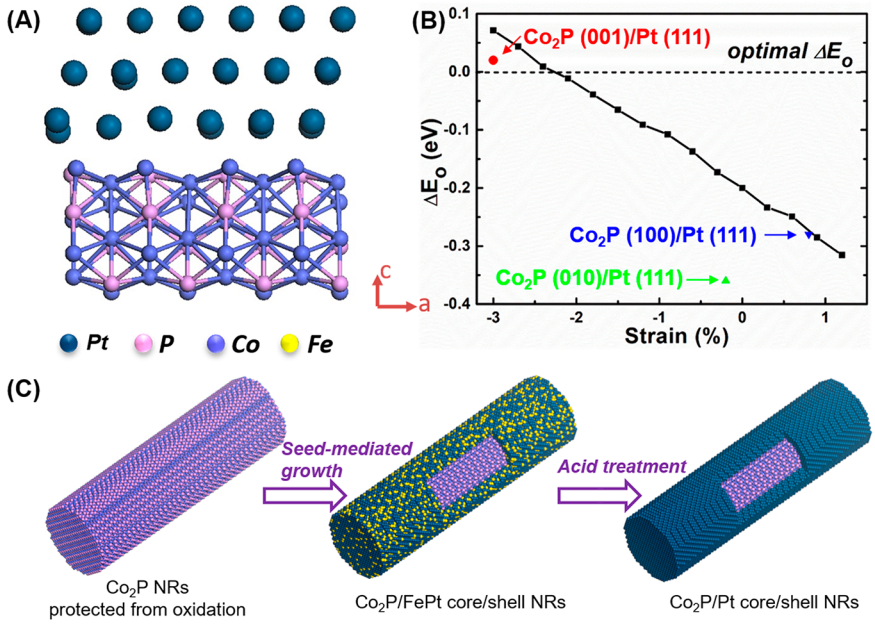

Figure 1. (A) Atomistic model of $Co_2P(001)/Pt(111)$ interface for DFT calculation. (B) DFT calculation results of different Co_2P/Pt interfaces: the black curve shows ΔE_O as a function of strain on Pt(111) surface. The negative (positive) percent strain means compressive (expansive) strain. The red, green, and blue dots correspond to ΔE_O values for $Co_2P(001)/Pt(111)$, $Co_2P(010)/Pt(111)$, and $Co_2P(100)/Pt(111)$ interfaces, respectively. The positive values of strain indicate tension strain, while the negative values indicate compression strain. The horizontal dashed line indicates the optimal ΔE_O value. (C) Schematic illustration of the seed-mediated growth to Co_2P/Pt core/shell NRs. The blue, purple, pink, and yellow spheres in (A) and (C) represent Pt, Co, P, and Fe atoms, respectively.

imposed by core material onto Pt shell due to their crystal lattice disparity.[15,36−38] Although the latter one is generally believed to be more dominant when Pt shell thickness exceeds two or three atomic layers,[39] the two effects tend to coexist and are difficult to be decoupled in core/shell NPs. More importantly, various interfaces are simultaneously formed within a core/shell NP in three dimensions, but it is very likely that only a few ones are beneficial to ORR catalysis, which is often oversimply interpreted or even overlooked. Therefore, such complexities make it challenging to predict what core/shell nanostructure is the most ideal catalyst for ORR. It is crucial to establish a "panoramic" understanding of core/shell interaction with the impact of each interface within the NP being comprehensively considered.

In this letter, we use Co_2P/Pt core/shell structure as an example to demonstrate that the favorable/unfavorable interfaces can be identified and controlled through designing and synthesizing low-dimensional core/shell nanostructures. Co_2P is chosen as a core material here because it is a nonprecious metal phosphide with the lattice constant close to Pt,[40] making it possible to uniformly grow a thin layer of Pt onto its surface without overly large interfacial energy. Meanwhile, in contrast to metallic materials that normally possess isotropic cubic crystal structure (e.g., Pt, Pd, Au, Fe, Co, Ni, and their alloys), its orthorhombic structure suggests its great potential to form anisotropic morphologies to expose specific facets.[40,41] If Co_2P core's dimensional anisotropy is rationally designed, we envision that a Co_2P/Pt core/shell nanostructure can be obtained with the desirable interfacial interactions being pronounced. Through density functional theory (DFT) calculations, we have screened a series of Co_2P/Pt interfaces and found that $Co_2P(001)/Pt(111)$ interface holds the best chance to optimize Pt energetics for ORR while $Co_2P(010)/Pt(111)$ will significantly decrease the activity of Pt. According to this prediction, we synthesize Co_2P NRs with a longitudinal direction of ⟨010⟩ to minimize its (010) plane in the surface. The subsequent seed-mediated growth can generate a core/shell Co_2P/Pt NRs with an ultrathin layer of Pt shell (≤1 nm). The produced Co_2P/Pt NRs with favorable $Co_2P(001)/Pt(111)$ interface expressed in the dominant side facets are highly efficient in catalyzing ORR in acid.

DFT calculations were performed to provide a deep understanding of the impact of Co_2P/Pt interfaces on surface Pt ORR activity (Supporting Information, SI). We have examined $Co_2P(001)/Pt(111)$, $Co_2P(010)/Pt(111)$, and $Co_2P(100)/Pt(111)$ interfaces as shown in Figures 1A and S1. The surface oxygen adsorption energies (E_O) based on these models were calculated to directly estimate the ORR activities over the three Co_2P/Pt interfaces. E_O has been widely used as a general descriptor for ORR kinetics, and there exists an optimal value of E_O for the maximum ORR rate.[42−44] Previous study has revealed that the optimal E_O is 0.2 eV higher than that on Pt(111) surface.[43,44] For comparison, we set the optimal E_O value at 0 eV and employ ΔE_O to represent the difference of a given E_O value relative to this optimal reference. Correspondingly, the negative ΔE_O (−0.2 eV) over unmodified Pt (111) surface demonstrates that an overbinding of oxygenated species on Pt surface, which can make the ORR kinetics sluggish. The results of ΔE_O for the three core/shell Co_2P/Pt interfaces are shown in Figure 1B. A catalyst with ΔE_O closer to zero is predicted to exhibit a higher ORR activity. Thus, the ORR performance of the three core/shell interfaces follow the order of $Co_2P(001)/Pt(111)$ > $Co_2P(100)/Pt(111)$ > $Co_2P(010)/Pt(111)$. Especially, $Co_2P(001)/Pt(111)$ displays a ΔE_O (0.02 eV), which is very close to the optimum ΔE_O, indicating its highly favorable nature for ORR catalysis. In contrast, $Co_2P(010)/Pt(111)$ with a ΔE_O of −0.36 eV is much worse than unmodified Pt(111) and should be

DOI: 10.1021/acs.nanolett.8b03666
Nano Lett. 2018, 18, 7870−7875

avoided in the fabrication of high performance ORR catalysts. In addition, the ΔE_O values are not significantly influenced by the termination of Co_2P surface (only 10 meV change with another termination) and the presence of P-vacancy at the Co_2P/Pt interfaces (less than 6 meV change) as shown in Figure S2.

For core/shell structures, in general both interfacial strain and ligand effects can influence the surface Pt's catalytic activity.[3,26,30−33,45,46] To understand the stand-alone strain effect, a flat Pt(111) surface is modeled under a lateral strain ranging from −3% (compression) to 1.2% (tension) with DFT and the results of ΔE_O are shown in Figure 1B, which reveal a linear relationship between the surface strain and ΔE_O. Therefore, any ΔE_O deviation of a core/shell structure to such a linear relationship is contributed by the ligand effect. As clearly seen, the strain and the ΔE_O of Co_2P(100)/Pt(111) fall exactly on the linear curve, indicating that the strain effect is dominant while the ligand effect can be negligible over Co_2P(100)/Pt(111) interface. This phenomenon can be explained when looking at the interface energies of these core/shell models. As summarized in Table S1, the interface energies ($E_{interface}$) of Co_2P(001)/Pt(111), Co_2P(010)/Pt(111), and Co_2P(100)/Pt(111) are calculated to be 975, 563, and 2171 mJ/m^2, respectively. A larger $E_{interface}$ over Co_2P(100)/Pt(111) implies a weaker binding between Pt shell and Co_2P core and thus diminishes the ligand effect on the ORR activity. The ligand effect becomes evident over Co_2P(010)/Pt(111) and Co_2P(001)/Pt(111) interfaces, which strengthens the surface Pt−O binding and make ΔE_O lower comparing to that predicted by strain effect. As a result, Co_2P(010)/Pt(111) is highly detrimental to ORR catalyst due to its strong ligand effect. Because of the favorable coupling between strain and ligand effects, the original positive ΔE_O value due to the "over-compressed" Pt strain in Co_2P(001)/Pt(111) can be negatively shifted and ultimately get very close to the optimum ΔE_O (0 eV).

Guided by the theoretical results, we target to synthesize Co_2P/Pt core/shell nanostructures with detrimental Co_2P(010)/Pt(111) and favorable Co_2P(001)/Pt(111) interfaces ratios being rationally balanced. Such a structure was obtained by a controlled seed-mediated growth of Pt shell in the presence of the Co_2P NRs (Figure 1C; SI). Co_2P NRs were made through the thermal decomposition of cobalt acetate in the mixture of tributylphosphine (TBP), trioctylphosphine oxide (TOPO), benzyl ether (BE), and oleic acid (OAc), according to our previous reported method.[40] TBP and TOPO are used as stabilizers as well as the phosphor sources. The as-synthesized Co_2P NRs have an average length of 20 ± 4 nm and a width of 2 ± 0.5 nm, as shown in the transmission electron microscopy (TEM) images (Figure S3). Aberration corrected scanning TEM (AC-STEM) high-angle angular dark-field (HAADF) images indicate the Co_2P NRs are single crystals with a longitudinal growth direction along ⟨010⟩ and side facets perpendicular to ⟨001⟩ or ⟨100⟩ directions (Figures 2A,B & S4). Meanwhile, we measured each NR's contrast intensity profile, as shown in Figure S5, and found the uniform contrast distribution along ⟨001⟩ or ⟨100⟩ directions. Because our STEM HAADF image is Z-contrast image whose contrast is proportional to NR thickness, we can conclude that the cross section of NR is a rectangle with one plane perpendicular to electron beam and therefore its side facets are (001) and (100) planes. Using these Co_2P NRs as the cores to construct core/shell NPs can minimize the formation of unfavorable

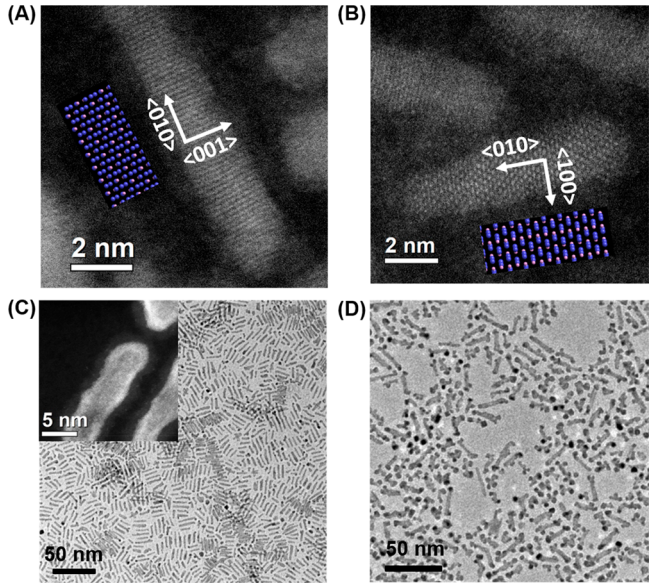

Figure 2. (A,B) STEM-HAADF images of the as-synthesized Co_2P NRs with their growth direction and structures identified. Insets in A and B illustrate the corresponding atomic models with purple and pink atoms being Co and P. (C,D) TEM image of Co_2P/FePt core/shell NRs (C) and branched NRs (D). Inset in C shows STEM-HAADF image of representative Co_2P/FePt core/shell NRs.

detrimental Co_2P(010)/Pt(111) interface as Co_2P (010) is only expressed at the NRs terminal.

Our previous study on Ni/FePt core/shell NPs have revealed that the seed-mediated growth of FePt would be prohibited once the seeding materials were oxidized.[36] Considering Co_2P is subject to the surface oxidation, we synthesized, purified, and well protected Co_2P NRs in N_2 atmosphere. The subsequent reduction of platinum acetylacetonate ($Pt(acac)_2$) and thermal decomposition of iron pentacarbonyl ($Fe(CO)_5$) allows the formation of uniform Co_2P/FePt NRs, as shown in the TEM image in Figure 2C. Control experiments indicate that FePt is prone to self-nucleation to NPs instead of coating the seeds, if using unprotected Co_2P NRs (Figure S6), similar to Ni/FePt NPs.[36] Besides, we notice that the addition of $Fe(CO)_5$ is necessary for the generation of core/shell structure. Without it, Pt tends to form cluster-like nanostructure without attaching to Co_2P (Figure S7). A possible reason to this phenomenon is that $Fe(CO)_5$ can release CO molecules which function to stabilize Co_2P against surface oxidation during the reaction as well as facilitate the Pt's uniform growth.[47]

The STEM-HAADF image in Figure 2C (inset) demonstrates that the obtained Co_2P/FePt NRs possess a uniform core/shell structure with a bright 0.6−1 nm shell being clearly visualized due to the higher Z-contrast of Pt comparing to Co and P (more images are shown in Figure S8). STEM-EELS 1D and 2D elemental mappings can further confirm the core/shell architecture as Co atoms exclusively concentrate in the core region and are encapsulated by a FePt polycrystal shell (Figures 3, S9, and S10). The formation of FePt can also be confirmed by X-ray diffraction (XRD) pattern shown in Figure S11 wherein the typical face-centered cubic FePt peaks and characteristic (111) peak can be observed. The peaks associated with Co_2P cannot be clearly manifested given the signal attenuation from Co being resonant with the Cu K-alpha source, which is consistent to the previous study on Co_2P NRs

DOI: 10.1021/acs.nanolett.8b03666
Nano Lett. 2018, 18, 7870−7875

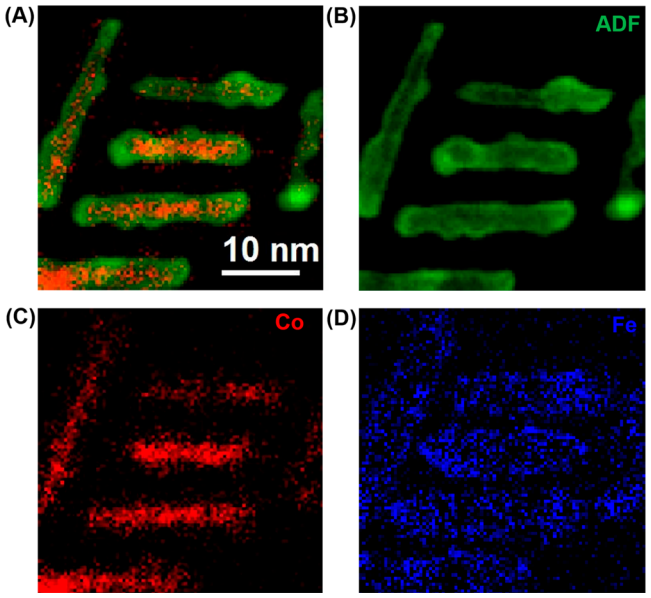

Figure 3. (A,B) STEM-HAADF image and (C,D) STEM-EELS 2D elemental mapping of Co, Fe on a group of as-synthesized Co_2P/FePt NRs.

and other Co and Ni-based NPs.[40,48] Interestingly, we find that to obtain a well-defined core/shell structure Co_2P seed/$Pt(acac)_2$ molar ratio needs to be carefully controlled. Decreasing this ratio can cause the production of branch-like structure and the branch density can be controlled (SI; Figures 2D and S12 show low-density and high-density branched NRs, respectively). The HAADF image in Figure S13 illustrates that FePt shell is still yielded while FePt branches are crystallographically cleaved to the shell, suggesting some FePt nuclei might form separately due to less amount of accessible seeds and then attach to core/shell Co_2P/FePt NRs. Similar oriented attachment has also been observed in other NR structures.[49]

To study the electrocatalytic property of NRs, we deposited the as-obtained Co_2P/FePt NRs or branched NRs on Ketjen carbon (C) support (denoted as C-NRs) and then treated them with glacial acetic acid (AA) at 70 °C for 12 h. This process can activate the catalyst surface by removing OAm and OAc hydrophobic ligands surrounding the NRs.[36] Thanks to the existence of compact Pt shell, NRs morphology is preserved (Figures 4A and S14) and Co_2P core is well protected in acid as demonstrated by unchanged Co/Pt atomic ratio before and after AA treatment. Meanwhile, Co_2P/FePt NRs evolve to Co_2P/Pt core/shell NRs because Fe positioning in the Pt shell can be etched in the course of AA treatment. These NRs samples' compositions were monitored by inductively coupled plasma-optical emission spectroscopy (ICP-OES) and summarized in Table S2. For core/shell NRs, only around 10% atomic ratio of Fe is detected in the shell after AA treatment. Improved Fe preservation is found in branched NRs, along with larger size FePt NPs branches being produced.

The C-NRs for ORR were evaluated in a standard three-electrode electrochemical system with rotating disk electrode (RDE). Figure 4B shows the cyclic voltammograms (CVs) of Co_2P/Pt NRs, commercial Pt (around 3 nm, Figure S15A) and PtCo alloy NPs (around 3 nm, Figure S15B) catalysts. It is clearly seen that the on-site potentials of OH_{ad} formation and

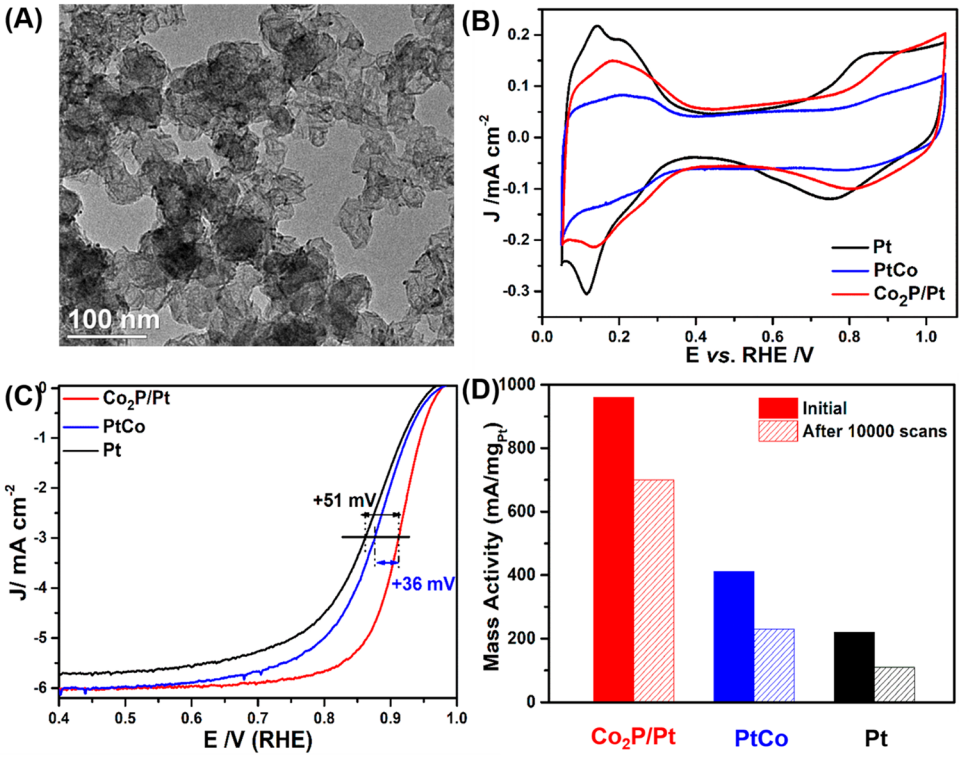

Figure 4. (A) TEM image of Co_2P/Pt core/shell NRs supported on C after AA treatment. (B) CVs of Co_2P/Pt core/shell NRs and commercial PtCo and Pt catalysts in N_2-saturated 0.1 M $HClO_4$. (C) ORR polarization curves of Co_2P/Pt core/shell NRs and commercial PtCo and Pt catalysts in O_2-saturated 0.1 M $HClO_4$ at 1600 rpm. (D) The mass activities of Co_2P/Pt core/shell NRs and commercial PtCo and Pt catalysts at 0.9 V before and after stability test.

DOI: 10.1021/acs.nanolett.8b03666
Nano Lett. 2018, 18, 7870−7875

Pt oxide reduction (E > 0.7 V vs RHE) are positively shifted in Co_2P/Pt and PtCo relative to pure Pt, implying their weaker bonding of Pt with oxygenated species.[50] Hydrogen underpotential formation/stripping peaks (H_{UPD}) (0.05−0.4 V) in CVs are used to estimate the electrochemically active surface areas (ECASAs) of the catalysts (Table S3). ORR polarization curves of these catalysts in O_2-saturated 0.1 M $HClO_4$ solution at 1600 rpm are displayed in Figure 4C. A positive shift of half-wave potential is clearly seen for Co_2P/Pt NRs compared with Pt (51 mV) and PtCo (36 mV), indicating the higher activity of Co_2P/Pt NRs than other two catalysts.[28] After normalizing over Pt mass, Co_2P/Pt NRs show a mass activity reaching 960 mA/mg_{Pt} at 0.9 V, superior to PtCo (410 mA/mg_{Pt}) and Pt (220 mA/mg_{Pt}) at the same condition. The specific activity follows the same trend, Co_2P/Pt (2.3 mA/cm^2) > PtCo (2.15 mA/cm^2) > Pt (0.31 mA/cm^2). After a stability testing of 10 000 scans with a potential range of 0.6−1.0 V, Co_2P/Pt NRs maintain their morphology and an activity at 700 mA/mg_{Pt}, whereas PtCo and Pt catalysts decrease to 230 and 110 mA/mg_{Pt}, respectively (Figures 4D and S16). The mass activity of Co_2P/Pt after stability testing is still much higher than our previous 0D Ni/Pt catalyst and U.S. Department of Energy 2020 target (440 mA/mg_{Pt}),[51] confirming that such 1D core/shell nanostructure does endow the catalyst with much enhanced performance.

The high performance of Co_2P/Pt NRs benefits from their completely nonprecious element core and 1D shape-induced minimization of detrimental $Co_2P(010)$/Pt(111) interface. Once forming branched structure shown in Figure 2D, the core/shell enhancement is evidently weakened. As demonstrated in Figures S17 and S18, branched NRs catalyst possesses an activity of 460 mA/mg_{Pt} and 1.6 mA/cm^2, much lower than uniform core/shell NRs. The decreased catalytic activity is associated with the fact that FePt branch energetics cannot be effective tuned by Co_2P core, as their interaction wanes rapidly in distance over several atomic layers.

In summary, we present for the first time the synthesis of 1D core/shell nanostructure with an ultrathin Pt shell and a nonprecious metal element core that can efficiently catalyze ORR in acid. The core/shell catalyst was constructed via a seed-mediated growth of FePt over Co_2P NRs and a subsequent acid washing that can convert FePt to Pt. Because of the 1D shape, such Co_2P/Pt NRs can effectively minimize the formation of $Co_2P(010)$/Pt(111) interface that is only formed at NRs terminals and highly detrimental to ORR catalysis as revealed by DFT calculation. Meanwhile, Pt surface energetics can be substantially improved by its favorable interaction with dominant side facet of underlaying Co_2P NRs. Especially, $Co_2P(001)$/Pt(111) interface provides a Pt−O binding energy very close to theoretical optimal value through an integrated strain and ligand effect, leading to much enhanced ORR activity of Co_2P/Pt NRs comparing with benchmark PtCo alloy and Pt NPs catalysts. The work highlights the importance of rational designing anisotropic nanostructures with favorable interfacial interactions to maximize the benefit of core/shell nanocatalysts.

■ ASSOCIATED CONTENT

Supporting Information

The Supporting Information is available free of charge on the ACS Publications website at DOI: 10.1021/acs.nanolett.8b03666.

Materials, synthesis, characterizations, electrochemical measurements, and DFT calculations. Table S1−S2. Figures S1−S16 (PDF)

■ AUTHOR INFORMATION

Corresponding Author

*E-mail: sz3t@virginia.edu.

ORCID

Zhiyong Zhang: 0000-0001-7936-9510
Xu Zhang: 0000-0002-6491-3234
Dong Su: 0000-0002-1921-6683
Jia X. Wang: 0000-0002-3947-9296
Sen Zhang: 0000-0002-1716-3741

Author Contributions

C.L. and Z.M. contributed to this work equally.

Notes

The authors declare no competing financial interest.

■ ACKNOWLEDGMENTS

This work was supported by U.S. National Science Foundation (DMR-1809700), Jeffress Trust Awards Program in Interdisciplinary Research from Thomas F. and Kate Miller Jeffress Memorial Trust and U.S. Department of Energy, Energy Efficiency and Renewable Energy, Fuel Cell Technology Office. Partial work on electron microscopy carried out at the Center for Functional Nanomaterials, Brookhaven National Laboratory, was supported by the U.S. Department of Energy, Office of Basic Energy Sciences, under Contract No. DE-SC-00112704.

■ REFERENCES

(1) Wu, J.; Yang, H. *Acc. Chem. Res.* **2013**, *46*, 1848−1857.
(2) Shao, M.; Chang, Q.; Dodelet, J. P.; Chenitz, R. *Chem. Rev.* **2016**, *116*, 3594−3657.
(3) Bing, Y.; Liu, H.; Zhang, L.; Ghosh, D.; Zhang, J. *Chem. Soc. Rev.* **2010**, *39*, 2184−2202.
(4) Li, D.; Wang, C.; Strmcnik, D. S.; Tripkovic, D. V.; Sun, X.; Kang, Y.; Chi, M.; Snyder, J. D.; van der Vliet, D.; Tsai, Y.; Stamenkovic, V. R.; Sun, S.; Markovic, N. M. *Energy Environ. Sci.* **2014**, *7*, 4061−4069.
(5) Guo, S.; Zhang, S.; Sun, S. *Angew. Chem., Int. Ed.* **2013**, *52*, 8526−8544.
(6) Chen, W.; Gao, W.; Tu, P.; Robert, T.; Ma, Y.; Shan, H.; Gu, X.; Shang, W.; Tao, P.; Song, C.; Deng, T.; Zhu, H.; Pan, X.; Yang, H.; Wu, J. *Nano Lett.* **2018**, *18*, 5905−5912.
(7) Kwon, H.; Kabiraz, M. K.; Park, J.; Oh, A.; Baik, H.; Choi, S.-I.; Lee, K. *Nano Lett.* **2018**, *18*, 2930−2936.
(8) Wang, X. X.; Hwang, S.; Pan, Y.-T.; Chen, K.; He, Y.; Karakalos, S.; Zhang, H.; Spendelow, J. S.; Su, D.; Wu, G. *Nano Lett.* **2018**, *18*, 4163−4171.
(9) Escudero-Escribano, M.; Malacrida, P.; Hansen, M. H.; Vej-Hansen, U. G.; Velázquez-Palenzuela, A.; Tripkovic, V.; Schiøtz, J.; Rossmeisl, J.; Stephens, I. E. L.; Chorkendorff, I. *Science* **2016**, *352*, 73−76.
(10) Chung, D. Y.; Jun, S. W.; Yoon, G.; Kwon, S. G.; Shin, D. Y.; Seo, P.; Yoo, J. M.; Shin, H.; Chung, Y.-H.; Kim, H.; Mun, B. S.; Lee, K.-S.; Lee, N.-S.; Yoo, S. J.; Lim, D.-H.; Kang, K.; Sung, Y.-E.; Hyeon, T. *J. Am. Chem. Soc.* **2015**, *137*, 15478−15485.
(11) Wang, D.; Xin, H. L.; Hovden, R.; Wang, H.; Yu, Y.; Muller, D. A.; DiSalvo, F. J.; Abruña, H. D. *Nat. Mater.* **2013**, *12*, 81−87.
(12) Wang, C.; Markovic, N. M.; Stamenkovic, V. R. *ACS Catal.* **2012**, *2*, 891−898.

DOI: 10.1021/acs.nanolett.8b03666
Nano Lett. 2018, 18, 7870−7875

(13) Wang, C.; Chi, M. F.; Li, D. G.; van der Vliet, D.; Wang, G. F.; Lin, Q. Y.; Mitchell, J. F.; More, K. L.; Markovic, N. M.; Stamenkovic, V. R. *ACS Catal.* **2011**, *1*, 1355−1359.
(14) Stamenkovic, V. R.; Mun, B. S.; Arenz, M.; Mayrhofer, K. J.; Lucas, C. A.; Wang, G.; Ross, P. N.; Markovic, N. M. *Nat. Mater.* **2007**, *6*, 241−247.
(15) Bu, L.; Zhang, N.; Guo, S.; Zhang, X.; Li, J.; Yao, J.; Wu, T.; Lu, G.; Ma, J. Y.; Su, D.; Huang, X. *Science* **2016**, *354*, 1410−1414.
(16) Lim, J.; Shin, H.; Kim, M.; Lee, H.; Lee, K.-S.; Kwon, Y.; Song, D.; Oh, S.; Kim, H.; Cho, E. *Nano Lett.* **2018**, *18*, 2450−2458.
(17) Beermann, V.; Gocyla, M.; Kühl, S.; Padgett, E.; Schmies, H.; Goerlin, M.; Erini, N.; Shviro, M.; Heggen, M.; Dunin-Borkowski, R. E.; Muller, D. A.; Strasser, P. *J. Am. Chem. Soc.* **2017**, *139*, 16536−16547.
(18) Huang, X.; Zhao, Z.; Cao, L.; Chen, Y.; Zhu, E.; Lin, Z.; Li, M.; Yan, A.; Zettl, A.; Wang, Y. M.; Duan, X.; Mueller, T.; Huang, Y. *Science* **2015**, *348*, 1230−1234.
(19) Stamenkovic, V. R.; Fowler, B.; Mun, B. S.; Wang, G.; Ross, P. N.; Lucas, C. A.; Marković, N. M. *Science* **2007**, *315*, 493−497.
(20) Wu, J.; Gross, A.; Yang, H. *Nano Lett.* **2011**, *11*, 798−802.
(21) Cui, C.; Gan, L.; Heggen, M.; Rudi, S.; Strasser, P. *Nat. Mater.* **2013**, *12*, 765−771.
(22) Choi, S.-I.; Xie, S.; Shao, M.; Odell, J. H.; Lu, N.; Peng, H.-C.; Protsailo, L.; Guerrero, S.; Park, J.; Xia, X.; Wang, J.; Kim, M. J.; Xia, Y. *Nano Lett.* **2013**, *13*, 3420−3425.
(23) Wu, J.; Qi, L.; You, H.; Gross, A.; Li, J.; Yang, H. *J. Am. Chem. Soc.* **2012**, *134*, 11880−11883.
(24) Li, M.; Zhao, Z.; Cheng, T.; Fortunelli, A.; Chen, C. Y.; Yu, R.; Zhang, Q.; Gu, L.; Merinov, B. V.; Lin, Z.; Zhu, E.; Yu, T.; Jia, Q.; Guo, J.; Zhang, L.; Goddard, W. A., III; Huang, Y.; Duan, X. *Science* **2016**, *354*, 1414−1419.
(25) Guo, S.; Li, D.; Zhu, H.; Zhang, S.; Markovic, N. M.; Stamenkovic, V. R.; Sun, S. *Angew. Chem., Int. Ed.* **2013**, *52*, 3465−3468.
(26) Chen, C.; Kang, Y.; Huo, Z.; Zhu, Z.; Huang, W.; Xin, H. L.; Snyder, J. D.; Li, D.; Herron, J. A.; Mavrikakis, M.; Chi, M.; More, K. L.; Li, Y.; Markovic, N. M.; Somorjai, G. A.; Yang, P.; Stamenkovic, V. R. *Science* **2014**, *343*, 1339−1343.
(27) Zhang, L.; Roling, L. T.; Wang, X.; Vara, M.; Chi, M.; Liu, J.; Choi, S.-I.; Park, J.; Herron, J. A.; Xie, Z.; Mavrikakis, M.; Xia, Y. *Science* **2015**, *349*, 412−416.
(28) Becknell, N.; Son, Y.; Kim, D.; Li, D.; Yu, Y.; Niu, Z.; Lei, T.; Sneed, B. T.; More, K. L.; Markovic, N. M.; Stamenkovic, V. R.; Yang, P. *J. Am. Chem. Soc.* **2017**, *139*, 11678−11681.
(29) Cai, B.; Hübner, R.; Sasaki, K.; Zhang, Y.; Su, D.; Ziegler, C.; Vukmirovic, M. B.; Rellinghaus, B.; Adzic, R. R.; Eychmüller, A. *Angew. Chem., Int. Ed.* **2018**, *57*, 2963−2966.
(30) Yang, X.; Roling, L. T.; Vara, M.; Elnabawy, A. O.; Zhao, M.; Hood, Z. D.; Bao, S.; Mavrikakis, M.; Xia, Y. *Nano Lett.* **2016**, *16*, 6644−6649.
(31) Strasser, P.; Koh, S.; Anniyev, T.; Greeley, J.; More, K.; Yu, C.; Liu, Z.; Kaya, S.; Nordlund, D.; Ogasawara, H.; Toney, M. F.; Nilsson, A. *Nat. Chem.* **2010**, *2*, 454−460.
(32) Hu, J.; Wu, L.; Kuttiyiel, K. A.; Goodman, K. R.; Zhang, C.; Zhu, Y.; Vukmirovic, M. B.; White, M. G.; Sasaki, K.; Adzic, R. R. *J. Am. Chem. Soc.* **2016**, *138*, 9294−9300.
(33) Ding, J.; Bu, L.; Guo, S.; Zhao, Z.; Zhu, E.; Huang, Y.; Huang, X. *Nano Lett.* **2016**, *16*, 2762−2767.
(34) Wang, X.; Choi, S.-I.; Roling, L. T.; Luo, M.; Ma, C.; Zhang, L.; Chi, M.; Liu, J.; Xie, Z.; Herron, J. A.; Mavrikakis, M.; Xia, Y. *Nat. Commun.* **2015**, *6*, 7594.
(35) Adzic, R. R.; Zhang, J.; Sasaki, K.; Vukmirovic, M. B.; Shao, M.; Wang, J. X.; Nilekar, A. U.; Mavrikakis, M.; Valerio, J. A.; Uribe, F. *Top. Catal.* **2007**, *46*, 249−262.
(36) Zhang, S.; Hao, Y.; Su, D.; Doan-Nguyen, V. V.; Wu, Y.; Li, J.; Sun, S.; Murray, C. B. *J. Am. Chem. Soc.* **2014**, *136*, 15921−15294.
(37) Luo, M.; Guo, S. *Nat. Rev. Mater.* **2017**, *2*, 17059.
(38) Zhang, S.; Zhang, X.; Jiang, G.; Zhu, H.; Guo, S.; Su, D.; Lu, G.; Sun, S. *J. Am. Chem. Soc.* **2014**, *136*, 7734−7739.
(39) Xie, S.; Choi, S.-I.; Lu, N.; Roling, L. T.; Herron, J. A.; Zhang, L.; Park, J.; Wang, J.; Kim, M. J.; Xie, Z.; Mavrikakis, M.; Xia, Y. *Nano Lett.* **2014**, *14*, 3570−3576.
(40) Doan-Nguyen, V. V.; Zhang, S.; Trigg, E. B.; Agarwal, R.; Li, J.; Su, D.; Winey, K. I.; Murray, C. B. *ACS Nano* **2015**, *9*, 8108−8115.
(41) Park, J.; Koo, B.; Yoon, K. Y.; Hwang, Y.; Kang, M.; Park, J.-G.; Hyeon, T. *J. Am. Chem. Soc.* **2005**, *127*, 8433−8440.
(42) Kulkarni, A.; Siahrostami, S.; Patel, A.; Nørskov, J. K. *Chem. Rev.* **2018**, *118*, 2302−2312.
(43) Nørskov, J. K.; Rossmeisl, J.; Logadottir, A.; Lindqvist, L.; Kitchin, J. R.; Bligaard, T.; Jonsson, H. *J. Phys. Chem. B* **2004**, *108*, 17886−17892.
(44) Greeley, J.; Stephens, I. E. L.; Bondarenko, A. S.; Johansson, T. P.; Hansen, H. A.; Jaramillo, T. F.; Rossmeisl, J.; Chorkendorff, I.; Nørskov, J. K. *Nat. Chem.* **2009**, *1*, 552−556.
(45) Cui, C.-H.; Yu, S.-H. *Acc. Chem. Res.* **2013**, *46*, 1427−1437.
(46) Li, H.-H.; Ma, S.-Y.; Fu, Q.-Q.; Liu, X.-J.; Wu, L.; Yu, S.-H. *J. Am. Chem. Soc.* **2015**, *137*, 7862−7868.
(47) Wang, L.; Zeng, Z.; Ma, C.; Liu, Y.; Giroux, M.; Chi, M.; Jin, J.; Greeley, J.; Wang, C. *Nano Lett.* **2017**, *17*, 3391−3395.
(48) Doan-Nguyen, V. V. T.; Kimber, S. A. J.; Pontoni, D.; Reifsnyder Hickey, D.; Diroll, B. T.; Yang, X.; Miglierini, M.; Murray, C. B.; Billinge, S. J. L. *ACS Nano* **2014**, *8*, 6163−6170.
(49) Zhang, Q.; Liu, S.-J.; Yu, S.-H. *J. Mater. Chem.* **2009**, *19*, 191−207.
(50) Wang, C.; Chi, M.; Li, D.; Strmcnik, D.; van der Vliet, D.; Wang, G.; Komanicky, V.; Chang, K. C.; Paulikas, A. P.; Tripkovic, D.; Pearson, J.; More, K. L.; Markovic, N. M.; Stamenkovic, V. R. *J. Am. Chem. Soc.* **2011**, *133*, 14396−14403.
(51) https://www.energy.gov/eere/fuelcells/doe-technical-targets-polymer-electrolyte-membrane-fuel-cell-components.

DOI: 10.1021/acs.nanolett.8b03666
Nano Lett. 2018, 18, 7870−7875